

# Nanoscale

Accepted Manuscript



This is an *Accepted Manuscript*, which has been through the Royal Society of Chemistry peer review process and has been accepted for publication.

*Accepted Manuscripts* are published online shortly after acceptance, before technical editing, formatting and proof reading. Using this free service, authors can make their results available to the community, in citable form, before we publish the edited article. We will replace this *Accepted Manuscript* with the edited and formatted *Advance Article* as soon as it is available.

You can find more information about *Accepted Manuscripts* in the [Information for Authors](#).

Please note that technical editing may introduce minor changes to the text and/or graphics, which may alter content. The journal's standard [Terms & Conditions](#) and the [Ethical guidelines](#) still apply. In no event shall the Royal Society of Chemistry be held responsible for any errors or omissions in this *Accepted Manuscript* or any consequences arising from the use of any information it contains.

**Efficient bulk heterojunction solar cells based on solution processed small molecules based on same benzo[1,2-b:4, 5-b']thiophene unit as core donor and different terminal units**

Challuri Vijay Kumar,<sup>a</sup> Lydia Cabau,<sup>a</sup> Emmanuel N. Koukaras,<sup>b,c</sup> Shahbaz .A. Siddiqui<sup>d</sup>, Ganesh D. Sharma\*<sup>d</sup> and Emilio Palomares\*<sup>a,e</sup>

<sup>a</sup>Institute of Chemical Research of Catalonia (ICIQ), Avda. Països Catalans 16, E-43007 Tarragona, Spain

<sup>b</sup>Institute of Chemical Engineering Sciences, Foundation for Research & Technology, Hellas, Stadiou Str. Platani, Patras, 26504, Greece

<sup>c</sup>Molecular Engineering Laboratory, Department of Physics, University of Patras, Patras, 26500 GR, Greece

<sup>d</sup>R & D Center for Engineering and Science, JEC group of Colleges, Jaipur Engineering College, Kukas, Jaipur 303101, India. E-mail: [gdsharma273@gmail.com](mailto:gdsharma273@gmail.com), and [sharmagd\\_in@yahoo.com](mailto:sharmagd_in@yahoo.com)

<sup>e</sup>Catalan Institution for Research and Advance Studies (ICREA), Avda. Lluís Companys 23, E-08010 Barcelona, Spain. E-mail: [epalomares@iciq.es](mailto:epalomares@iciq.es)

We report the synthesis, characterization, optical and electrochemical of two novel molecules **DRT3-BDT (1)** and **DTT3-BDT (2)** comprising of same BDT central core (donor) and different end capped acceptor units, i.e. rhodanine with ethyl hexyl and thiazolidione with ethylhexyl via linked an alkyl-substituted terthiophene (3T)  $\pi$ -conjugation bridge, respectively. Electrochemical properties of these small molecules indicate that their energy levels are compatible with energy levels of PC<sub>71</sub>BM for efficient exciton dissociation. These molecules have been used as electron donor along with PC<sub>71</sub>BM as electron acceptor for the fabrication of solution processed “small molecule” bulk heterojunction (BHJ) solar cells (smOPV). The device prepared from optimized **1**:PC<sub>71</sub>BM(1:1) processed cast from DIO (3%v)/CF solvent exhibited a power conversion efficiency of 6.76 % with  $J_{sc} = 11.92$  mA/cm<sup>2</sup>,  $V_{oc} = 0.90$  and FF = 0.63. The device with **2**:PC<sub>71</sub>BM under same conditions showed a lower PCE of 5.25 % with  $J_{sc} = 10.52$  mA/cm<sup>2</sup>,  $V_{oc} = 0.86$  and FF = 0.56. The AFM, TEM and PL quenching measurements revealed that the high  $J_{sc}$  is a result of the appropriate morphology and exciton dissociation. The performances comparison of devices based on two small molecules, the higher  $J_{sc}$  for device **1** was attributed to its better nanoscale phase separation, smooth surface and higher carrier mobility in the **1**:PC<sub>71</sub>BM blend film. Moreover, the higher value of FF for the **1**:PC<sub>71</sub>BM based device was ascribed to a good balance between the electron and hole mobilities.

\* Corresponding authors

## 1. Introduction

In the last two decades, organic solar cells based on bulk heterojunction (BHJ) active layer have drawn lot of attention because of their advantages in lightweight, flexibility and simple manufacturing process and would be one of the promising technologies for future energy harvesting [1-7]. Although the polymer based donor materials are one of the important components in organic BHJ solar cells [8-13], where they have used as donor along with fullerene as acceptor in active layer and power conversion efficiency (PCE) over 9 % has been reported [14-18]. The so called “small molecules” based donor materials are an interesting alternative offering several promising advantages over their polymer counterparts, including monodispersity and well defined molecular structure, easy purification, and better reproducibility (less batch to batch variation) [19-25] and a PCE in the range 8-10 % has been achieved in recent years for a single junction solar cells [26-28] and a PCE of 10.1 % for tandem cell devices [29].

In most of the BHJ organic solar cells based on solution processed small molecule as donor showed relatively low fill factor (FF) and short circuit current ( $J_{sc}$ ) as compared their polymer counterparts, due to their poorer film formation ability [30]. At present, different kinds of solution processed small molecules with wide absorption, high hole mobility, as well as appropriate miscibility with fullerene derivative acceptor to form uniform interpenetrating networks, have been developed for high efficiency small molecule BHJ solar cells. In particular, the most promising small molecule donor materials for BHJ solar cells are normally designed by connecting various electron donating (D) and electron withdrawing (A) moieties through a  $\pi$ -conjugating spacer i.e. (D- $\pi$ -A) structure [31-37]. Such a D- $\pi$ -A structure can be used to lower the optical bandgap to broaden the optical absorption profile and to assist the formation of favorable morphologies for efficient small molecule BHJ organic solar cells. Among the different small molecule with A-D-A structure for organic solar cells, benzo[1,2-b:4,5-b']-dithiophene (BDT) derivatives has been proved to be a promising materials for photovoltaic applications [38-40]. The incorporation of thiophene side chains could extend the vertical  $\pi$ - $\pi$  conjugation and promote  $\pi$ - $\pi$  stacking in the solid state [41, 42] and thereby improving the charge transport, leading to an enhancement in corresponding  $J_{sc}$  [43]. In the case of 2D BDT based polymer solar cells, demonstrated high  $V_{oc}$  as compared to one dimensional (1D) BDT counterparts, due to its deeper highest occupied molecular orbital (HOMO) energy levels [44, 45] and showed excellent photovoltaic performance with PCEs of over 7 % [41, 46]. The BDT unit a symmetric and

coplanar conjugated structure, and most importantly, it can be relatively easily modified and it exhibit good electron delocalization and excellent hole mobilities. Chen and coworker reported a 2D BDT small molecule, DR3TBDT, that demonstrated a PCE of 8.12 % [21]. Recently, Chen et al. designed and synthesized a new A-D-A small molecule with BDT as central donor core, namely DR3TSBDT for solution processed BHJ organic solar cells and achieved a record PCE of 9.95 % [28]. These research work also revealed that the nature of the acceptor end group mainly influence the performance of the resulting SMOPV. Hence to enhance light absorption and to tune the HOMO energy level, lot of effort has been put to design the new acceptor units.

A small molecule featuring an electron donating central core,  $\pi$ -conjugated spacers, and electron accepting end caps could be suitable for the preparation of the solution processed organic solar cells. In such systems, cyanoacetate, and rhodamine acceptors have been employed in conjugation with different central donor cores, including benzodithiophene [47, 48], dithienosiole [49, 50] and benzotriphiphenylene [51]. Chen et al. have recently designed a small molecule containing 4,8-dioctyl benzo[1,2-b:4,5-b']dithiophene as the central block and 3-(2-ethylhexyl)-rhodanine as the end-capping groups and achieved a PCE of 8.26 % through the active layer optimization process combining thermal and solvent vapor optimization [52]. Sun et al have designed a new small molecule donor benzodithiophene terthiophene rhodanine (BTR) and achieved a excellent PCE of 9.3 % [53].

Recently, we have designed as small molecule with BDT donor core and 3-ethyrodanine as electron withdrawing end groups linked through cyclopentadithiophene  $\pi$  spacer and used it as donor component along with PC<sub>71</sub>BM as acceptor component for solution processed BHJ solar cells and achieved a PCE of 6.07 % after the optimization of solvent additive [54]. In continuation of our research work on the designing of new novel small molecules based on BDT core, in this study, we have synthesized two A-D-A small molecules, denoted as **DRT3-BDT (1)** and **DTT3-BDT (2)** comprising of same BDT as central core (donor) and different end capped acceptor units, i.e. rhodanine with ethyl hexyl and thiazolidione with ethylhexyl via linked an alkyl-substituted terthiophene (3T)  $\pi$ -conjugation bridge. These small molecules were used as donor along with PC<sub>71</sub>BM acceptor for the fabrication of solution processed small molecule BHJ organic solar cells. The devices based on **1**:PC<sub>71</sub>BM (1:1) and **2**:PC<sub>71</sub>BM (1:1) processed with DIO (3%v)/CF exhibit PCE of 6.76 % and 5.26 %, respectively.

## 2. Experimental details

## Synthesis and characterization of small molecules

The synthesis of small molecule 1 and 2 and their detail characterization were given in the supplementary information.

### 2.1 Device fabrication and characterization

The small molecule BHJ solar cells were prepared as follows: First ITO coated glass substrate was cleaned by detergent powder, acetone and isopropyl alcohol with ultrasonication. After drying the cleaned ITO substrate in ambient atmosphere, the hole transport material of PEDOT:PSS (Clevious PH) was spin-coated at 3000 rpm for 40 s to obtain the film thickness of 40 nm. The **1** or **2**: PC<sub>71</sub>BM (donor : acceptor) blend solution was prepared from different weight ratio of 1:0.5, 1:1 and 1:1.5 and total concentration of 20 mg/mL in chloroform (CF) with 1, 2, 3 and 4 v % of 1,8 -diodooctane (DIO) processing additive. After stirring overnight at 50°C, the blend was heated to 80° C for 15 min before spin casting. The photoactive layer was obtained from spin casting the solution at 2000-2500 rpm for 60 min and then the film was dried at 60° C for 10 min to evaporate residual solvent. The thickness of the active layer was controlled by the spinning speed during the spin coating of active layer and was in the range of 90-100 nm. Finally, the aluminum (Al) top electrode was thermally deposited on the active layer at a vacuum of 10<sup>-5</sup> Torr through a shadow mask of area of 20 mm<sup>2</sup>. All devices were fabricated and tested in ambient atmosphere without encapsulation. The hole-only and electron-only devices with ITO/ PEDOT:PSS / **1** or **2**:PC<sub>71</sub>BM/ Au and ITO/ Al/**1** or **2**:PC<sub>71</sub>BM/ Al architectures were also fabricated in an analogous way, in order to measure the hole and electron mobility, respectively. The current-voltage characteristics of the BHJ organic solar cells were measured using a computer controlled Keithley 238 source meter under simulated AM1.5G, 100 mW/cm<sup>2</sup>. A xenon light source coupled with optical filter was used to give the stimulated irradiance at the surface of the devices. The incident photon to current efficiency (IPCE) of the devices was measured illuminating the device through the light source and monochromator and the resulting current was measured using a Keithley electrometer under short circuit condition.

## 3. Results and discussion

### 3.2 Synthesis and characterization of small molecules

The chemical structures of **DRT3-BDT (1)** and **DTT3-BDT (2)** is shown in scheme 1. The synthetic route of two new small molecules **DRT3-BDT (1)** and **DTT3-BDT (2)** based on benzodithiophene with different end group acceptors. **DRT3-BDT (1)** and **DTT3-BDT (2)** consisting the 5',5''''- (4,8-bis (5-(2-ethylhexyl)thiophen-2-yl) benzo [1,2-b:4,5-b']

dithiophene-2,6-diyl) bis (3,3''-dioctyl-[2,2':5',2''-terthiophene]-5-carbaldehyde) (**7**) as donor and 3-ethyl hexyl rhodanine and 3-ethylhexyl thiazolidine-2,4-dione with octyl terthiophene as a bridge is shown in Scheme 2. The synthesis of BDT (**7**) building block synthesized according to the reported procedure [21]. These two acceptors synthesized via the potassium salt of rhodanine and thiazolidine-2,4-dione reacted with ethylhexyl bromide in the presence of potassium iodide with the solvent of acetone and DMF. The targeted molecules were prepared the Knoevenagel condensation with BDT (**7**) with 3-ethyl hexyl rhodanine and 3-ethylhexyl thiazolidine-2, 4-dione, respectively. To obtain the best possible performance in OSC devices **DRT3-BDT (1)** and **DTT3-BDT (2)** was purified by consecutive flash chromatography, size exclusion chromatography. This combination of techniques was found effective in removing most of the impurities. Both the small molecules are soluble in common organic solvents. The important intermediates and targeted molecules were characterized by the  $^1\text{H-NMR}$ ,  $\text{C}^{13}\text{-NMR}$ , MALDI-TOF and with elemental analysis (for detail see the [supporting](#) information).

### 3.1 Optical and electrochemical properties

Figure 1a and 1b shows the absorption spectra of compounds in dilute chloroform solution and thin film cast from chloroform solvent, respectively. The absorption spectra of both small molecules in solution are identical and exhibits one main peak around 506 nm and 492 nm for **DRT3-BDT (1)** and **DTT3-BDT (2)**, respectively, which is attributed to the intramolecular charge transfer (ICT) between the donor and acceptor units present in the small molecules, other smaller peaks at shorter wavelengths could be assigned to the  $\pi\text{-}\pi^*$  transitions. As compared to the absorption spectra of these small molecules, the thin film, the spectrum was broaden and redshift with maximum absorption at wavelength around 576 nm and 556 nm for **1** and **2**, respectively. In addition, a vibronic shoulder peak at 632 nm and 606 nm for **1** and **2**, respectively was observed, which indicates effective  $\pi\text{-}\pi$  stacking between molecule backbones. The optical bandgap estimated from the onset of absorption is about 1.74 eV and 1.84 eV for **1** and **2**, respectively.

The cyclic voltammetry (as shown in Figure 2a and 2b) was used to estimate of the HOMO and LUMO energy levels of the small molecules. The potentials were internally calibrated using the ferrocene /ferrocenium ( $\text{Fc}/\text{Fc}^+$ ) redox couple (4.4 eV below the vacuum level). The estimated values of the HOMO and LUMO energy levels are compiled in table 1. The HOMO levels of the both the small molecule is same (-5.42 eV and -5.38 eV for **1** and **2**) but the LUMO levels are different (-3.54 eV and -3.44 eV, respectively), attributed to the

same core donor (BDT) and different acceptors in the small molecules, since the HOMO energy level in D-A molecule depends upon the donor, while LUMO energy level decided by the type of acceptor. The electrochemical bandgap is estimated to be about 1.88 and 1.94 eV for **1** and **2**, respectively, which are in agreement with the optical bandgap. The deeper level of HOMO these small molecules could generate high values of  $V_{oc}$  in BHJ organic solar cells.

### 3.2 Theoretical Calculations

We have additionally performed a theoretical study on the **1** and **2** molecular structures within the framework of density functional theory (DFT) and time-dependent density functional theory (TD-DFT). The initial geometry optimization calculations were performed employing the gradient corrected functional PBE [55] of Perdew, Burke and Ernzerhof. The def-SVP basis set [56], was used for all of the calculations. At this stage of the calculations, to increase the computational efficiency (without loss in accuracy), the resolution of the identity method [57, 58] was used for the treatment of the two-electron integrals. Subsequent geometry optimization were further performed using the hybrid exchange–correlation functional B3LYP [59] as well as Truhlar’s meta-hybrid exchange–correlation functional M06 [60], and the same basis set. Tight convergence criteria were placed for the SCF energy (up to  $10^{-7}$  Eh) and the one-electron density (rms of the density matrix up to  $10^{-8}$ ) as well as for the norm of the Cartesian gradient (residual forces both average and maximum smaller than  $1.5 \times 10^{-5}$  a.u.) and residual displacements (both average and maximum smaller than  $6 \times 10^{-5}$  a.u.). Solvent effects were included for chloroform (CF) using the integral equation formalism variant of the Polarizable Continuum Model (IEFPCM), as implemented in the Gaussian package [61].

TD-DFT excited state calculations were performed to calculate the optical gap of the **1** and **2** molecules using the same functionals and basis set on the corresponding ground state structures. The UV/Vis spectra were calculated using the B3LYP and M06 functionals. The first round of geometry optimization was performed using the Turbomole package [62]. All of the follow up calculations were performed using the Gaussian package [61].

For the geometry optimization of the **1** molecular structure several rotamers were examined as initial geometries, including aliphatic configurations. We performed vibrational analysis on the energetically lowest optimized structure and found it to be a true local (if not global) minimum; none of the vibrational modes had imaginary eigen frequencies. The two structures of lowest energy were suitably modified and used as initial geometries of the **2** structure for the corresponding geometry optimizations. In this case as well vibrational analysis on the final, energetically lowest, structure revealed no imaginary eigen frequencies.

The backbone of the structures, i.e. the chain of ring units, is highly planar, with average dihedral angles between neighboring rings in around  $12^\circ$ . The dihedral angles between the edge thiazolidine- groups are in the range of  $11^\circ$ – $15^\circ$  for **1** and  $13^\circ$ – $17^\circ$  for **2**, depending on the functional used and the presence of solvent. We have calculated the HOMO and LUMO energy levels and the optical gaps, defined here as the energetically lowest allowed vertical electronic excitation, employing the PBE, M06, and B3LYP functionals. In Table 1, in addition to the frontier orbitals' energy levels, we also provide the optical gap the main contributions to the first excitation as well as the wavelength of the first excitation and of the excitations with the largest oscillator strengths.

In addition to the B3LYP functional we have also performed our calculations employing the M06 functional. The M06 meta-hybrid functional was chosen since it provides leveled performance over transition types [62, 63]. We provide results using all three functionals, which can additionally be used for comparison with the literature.

We find, as expected, that the PBE functional underestimates both the HOMO–LUMO (HL) and the optical gaps. The HL gap calculated using the hybrid B3LYP functional is about 0.35 eV smaller than that using the meta-hybrid M06 functional, however, for the calculated optical gaps this difference is smaller, about 0.15 eV, with the later in better agreement to experiment value for the optical gap. In Table 1, we also provide the character of the first allowed excitations only for contributions larger than 4%. The first excitation, as calculated by the PBE and B3LYP functionals, exhibits a single-configuration character, while for the meta-hybrid functional M06, with moderate secondary contributions are also noted.

In Figure 3, we have plotted the isosurfaces (isovalue=0.02) of the HOMO and LUMO, as well as the next nearest frontier orbitals that take part in transitions that contribute to the first excitation, of the **1** and **2** structures. For both structures the HOMO extends over the main, nearly planar, body of the structures, with very small contributions from the edge thiazolidine- (**TAD** and **TADO**) groups. The LUMO on both structures seems to be localized on the terthiophene (**TT**) chains and the edge thiazolidine- groups with very small contributions from the central part (dithiophenylbenzodithiophene) (**DTBDT**) of the structures. This partitioning is even more pronounced for LUMO+1. For LUMO+2 this may seem reversed, since it is localized on both the central and edge part of the structures. However, by examining the contribution to the first excitation the transition to LUMO+2 is from HOMO which displays greater localization in central region. To quantify the contributions of the moieties to the frontier orbitals we have calculated the total and partial

density of states (PDOS). The PDOS for **1** and **2** is shown in Figure 4. We partition **1** into the **TAD**, **TT**, **DTBDT**, and the aliphatic groups. Similar for **2** with but instead of **TAD** we denote **TADO** for the –dione oxygens. For the **1** structure the contribution of the **BTBDT**, **TT**, and **TAD** groups to the HOMO is 39.7%, 53.2%, and 5.6% respectively, with only a 1.4% combined contribution from all the aliphatic groups. The corresponding contributions to the LUMO are 7.1%, 58.7% and 33.6%, respectively, and 0.6% combined from all the aliphatic groups. This is in agreement with our earlier observation on the localization of HOMO on the inner structure and the LUMO mainly on the outer structure. The first significant contributions (7.0%) from the aliphatic groups are noted at lower energies, around –7.4 eV which corresponds to the HOMO–13 level. For the **2** structure the contribution of the **BTBDT**, **TT**, and **TADO** groups to the HOMO is 42.8%, 51.0%, and 4.7% respectively, with only a 1.4% combined contribution from all the aliphatic groups. The corresponding contributions to the LUMO are 11.1%, 64.4% and 23.6%, respectively, and 0.8% combined from all the aliphatic groups. The first significant contributions (6.9%) from the aliphatic groups are noted at lower energies, around –7.52 eV which corresponds to the HOMO–13 level.

In Figure 5, we show the UV/Visual absorption spectra of the **1** and **2** structures calculated at the TD-DFT/M06 level of theory, both accounting for solvent effects for CF and in gas phase. The spectra have been produced by convoluting Gaussian functions with HWHM = 0.20 eV centered at the excitation wavenumbers. In Figure S13 (see Supporting Information) we also provide the corresponding spectra calculated using the B3LYP functional, which has somewhat overestimated wavenumbers compared to both the calculated with M06 and the experimental spectra. The low energy band calculated using M06 is overestimated by about 80 nm. The absorption spectra of both structures display three main bands in the visual region that cover a wide spectral range.

A characteristic three band absorption spectrum is found that displays a main band centered at 613 nm for **1** and 574 nm **2**, and two lower intensity bands at smaller wavelengths, specifically centered at 488 nm and 340 nm for **1**, and 445 nm and 324 nm for **2**. The calculated spectrum is slightly overestimated compared to the available region of the experimental one by about 75 nm. The wavelengths of the excitations with the largest oscillator strengths within these bands are given in Table 1.

Figure 6 shows the absorption spectra of **1**:PC<sub>71</sub>BM and **2**:PC<sub>71</sub>BM blend (optimized ratio 1:1 for the best performance BHJ organic solar cells) thin film with and without DIO additives. The normalized absorption bands observed in **1** or **2**:PC<sub>71</sub>BM BHJ films without

and additive exhibited spectral characteristics similar to that of their pristine solid state film, but the peak intensities of their vibronic shoulders were slightly disappeared. However, these shoulder peaks reappear with the addition of additive, indicating that additive affected effectively the intermolecular  $\pi$ - $\pi$  packing interaction of these small molecules in the blend morphology [65].

### 3.3 Photovoltaic properties

The organic solar cells were fabricated using the blends of these solution processed small molecules as electron donors along with PC<sub>71</sub>BM as acceptor with a conventional device structure of ITO/PEDOT:PSS/ **1** or **2**:PC<sub>71</sub>BM/Al. First of all we have optimized the weight ratio of donor (**1** or **2**) to acceptor (PC<sub>71</sub>BM) for CF cast blend and found the optimized ratio was 1:1. Then we have varied the solvent additive (DIO) concentration and found optimized volume ratio was 97:3 (CF/DIO). The **1** or **2**:PC<sub>71</sub>BM blends were dissolved in a optimized mixed solvent containing CF and 1,8-diiodooctane (DIO) in volume ratio of 97:3. Devices prepared using either small molecule showed the best performances for **1** or **2**:PC<sub>71</sub>BM blend ratio of 1:1. The best current –voltage (J-V) characteristics of the devices, under the illumination of AM1.5 G, 100 mW/cm<sup>2</sup> are displayed in Figure 7a, and corresponding photovoltaic parameters are compiled in table. With optimized weight ratio of **1** or **2** to PC<sub>71</sub>BM at 1:1 (processed with 3 %v DIO/CF), the device based on **1**:PC<sub>71</sub>BM showed a PCE of 6.76 % with J<sub>sc</sub>=11.92 mA/cm<sup>2</sup>, V<sub>oc</sub>=0.90 V and FF= 0.63. In contrast the device based on **2**:PC<sub>71</sub>BM showed lower PCE of 5.25% with a J<sub>sc</sub> =10.52 mA/cm<sup>2</sup>, V<sub>oc</sub>=0.86 V and FF=0.58. The devices based on **1** and **2** displayed high V<sub>oc</sub>, considering their deeper HOMO energy levels. The higher value of PCE for **1**:PC<sub>71</sub>BM when compared to **2**:PC<sub>71</sub>BM, under identical conditions, is attributed to the larger value of J<sub>sc</sub> and FF and also consistent with the higher values of IPCE (Figure 7b). The absorption spectrum (Figure 6) of the blends clearly showed that the photons absorbed by **1**:PC<sub>71</sub>BM is higher than that of **2**:PC<sub>71</sub>BM resulting in higher J<sub>sc</sub>. The higher value of FF for device based on **1** as compared to the **2** is attributed to a decrease of series resistance (R<sub>s</sub>) as measured from the slope of the forward J-V characteristics under illumination around the V<sub>oc</sub>, and by an increase of shunt resistance (R<sub>sh</sub>), as derived from the slope of J-V characteristics in the third quadrant.

The IPCE curves of the devices based on the **1** and **2** are shown in Figure 7b. The IPCE spectra closely resembles with the absorption spectra of the corresponding layers. Obviously, both small molecules **1** and **2** contribute in longer wavelength region and PC<sub>71</sub>BM contribute more in shorter wavelength region. Under the same experimental conditions, IPCE

values for device based on **1** is higher than that for the device based on **2** in good agreement to the larger value of  $J_{sc}$  for **1**. The higher value of  $J_{sc}$  and FF may also be attributed to the higher hole mobility for **1**:PC<sub>71</sub>BM blend and broader absorption profile of **1**:PC<sub>71</sub>BM blend. The integrated value of  $J_{sc}$  from the IPCE spectra of the device based on **1** and **2** are 11.80 mA/cm<sup>2</sup> and 10.42 mA/cm<sup>2</sup>, respectively. These values are in agreement with the experimental values of  $J_{sc}$ .

It was reported that optimal BHJ morphologies consists of interpenetrating bicontinuous nanoscale domains (15-20 nm) of each donor and acceptor components, on the order of exciton diffusion length, which extend vertically from each electrode, thereby increasing the surface area D-A interface and forming continuous conducting pathways for efficient exciton dissociation, charge transfer and extraction [66-70]. To understand the information about the higher  $J_{sc}$  and FF for the device based on **1**, as compared to **2**, we have investigated the morphology of the active layers, exciton dissociation efficiency, and charge carrier mobilities in the small molecules and small molecules :PC<sub>71</sub>BM films. The film morphologies were investigated using TEM and AFM. The TEM images of the small molecule:PC<sub>71</sub>BM are shown in Figure 8. Both the films showed nanoscale phase separation while **1**:PC<sub>71</sub>BM blend exhibit more homogeneous nanoscale phase separation than that **2**:PC<sub>71</sub>BM. AFM images of small molecule: PC<sub>71</sub>BM blend films are shown in Figure 9. AFM images of both the film showed smooth surfaces while the roughness of **1**:PC<sub>71</sub>BM film (rms = 1.25 nm) was lower than that for **2**:PC<sub>71</sub>BM film (rms= 1.90 nm).

Photoluminescence (PL) spectra of pristine small molecules and their blends with PCBM thin films cast from THF and DIO/CF was measured to get more information about the exciton dissociation efficiency in the devices. Figure 10 shows the PL spectra of small molecules and **1** or **2**:PC<sub>71</sub>BM blends spin cast from THF or DIO/CF solvents. **1** and **2** showed PL with peak at around 618 nm and 708 nm, respectively. Blending upon PC<sub>71</sub>BM with small molecule significantly quenched the PL. The quenching is more effective with the addition of DIO. This effective quenching indicates that the exciton dissociation was efficient in both blend films. More effective quenching in the **1**:PC<sub>71</sub>BM than **2**:PC<sub>71</sub>BM blend attributes to two possibilities: (i) better exciton dissociation efficiency in the **1**:PCBM blend film and (ii) larger interfacial area between small molecule and PC<sub>71</sub>BM through more optimal nanoscale phase separation. The former possibility may be possible because the **1** had a higher LUMO energy level than **2**. The latter was mainly responsible for effective PL quenching, as confirmed from the morphological measurements. From the morphology and

PL studies, we conclude that **1**:PC<sub>71</sub>BM active layer has more favorable features for higher  $J_{sc}$ .

The hole mobility is another important factor for OSCs, because it influences the charge transport in the device. High hole mobility and balance between the electron and hole mobilities of BHJ active layer is necessary for effective charge carrier transport to the electrodes and also reduce the photocurrent loss in the OSCs. The hole and electron mobilities were measured by space charge limited current (SCLC) method with a device structure of ITO/PEDOT:PSS/**1** or **2**:PC<sub>71</sub>BM/Au (hole only) and ITO/Al/**1** or **2**:PC<sub>71</sub>BM/Al (electron only), respectively. We have also measured the hole mobilities for pristine small molecules also. The current density (JSCLC) in SCLC region is described by following expression:

$$J_{SCLC} = \frac{9}{8} \epsilon_0 \epsilon_r \mu \frac{V^2}{L^3}$$

Where  $\epsilon_0$  is the permittivity of free space,  $\epsilon_r$  is the relative dielectric constant of the transport medium,  $\mu$  is the charge carrier mobility (hole and electron for hole only device and electron only device, respectively),  $V = V_{app} - V_{bi}$ , ( $V_{app}$  and  $V_{bi}$  is applied voltage and built in potential) is the internal potential in the device and  $L$  is the thickness of the active layer. The current–voltage characteristics for the hole only devices in dark were shown in Figure 11. As shown in Figure 11, according to above expression, the hole mobility was calculated to be  $8.68 \times 10^{-5}$  and  $2.94 \times 10^{-5}$  cm<sup>2</sup>/Vs for **1** and **2**, respectively. Although the electron mobility for both the active layers (estimated from J-V characteristics of electron only device shown in Figure S14) either with **1** or **2** was almost same i.e.  $2.56 \times 10^{-4}$  cm<sup>2</sup>/Vs, since the electron mobility is dominated by acceptor molecule (PC<sub>71</sub>BM). Therefore the ratio between the electron and hole mobilities for the devices based on **1** and **2** are about 2.95 and 8.71, respectively, leading to the better charge transport in the device based on **1**, as compared to **2**, resulting higher values of  $J_{sc}$ , FF and PCE.

To get information about the exciton generation and dissociation behaviors, in these solar cells based on **1** and **2**, we have evaluated the maximum photoinduced carrier generation rate per unit volume ( $G_{max}$ ) and charge collection probability ( $P_c$ ) in these devices. The devices were biased swept from -1 V to 1 V. Figure 12 shows the variation of photocurrent ( $J_{ph}$ ) with effective voltage ( $V_{eff}$ ) for devices based on **1** and **2** small molecules, measured under illumination at 100 mW/cm<sup>2</sup>.  $J_{ph}$  is defined as  $J_{ph} = J_L - J_D$ , where  $J_L$  and  $J_D$  are the current densities under illumination and under the dark.  $V_{eff}$  is defined as  $V_{eff} = V_o -$

$V_{app}$ ,  $V_o$  is the voltage, when  $J_{ph} = 0$  ( $J_L = J_D$ ), and  $V_{app}$  is the applied voltage [71]. Figure 12 shows the two distinct regions : (i)  $J_{ph}$  increases linearly at the low  $V_{eff}$ , and (ii)  $J_{ph}$  saturates at the high  $V_{eff}$ , in which the internal electric field is large enough to dissociate all the photogenerated excitons into free charge carriers and sweep out all the carriers to the electrodes. Therefore, at a high  $V_{eff}$ , the saturation photocurrent density ( $J_{ph, sat}$ ) is limited by the total number of absorbed photons, and assuming that  $J_{ph, sat}$  is independent of bias and temperature, we determined the  $G_{max}$ , using  $J_{ph, sat} = qLG_{max}$ , where  $q$  is the electronic charge and  $L$  in the thickness of the active layer used in the device [72]. The value of  $G_{max}$  for the devices based on **1** and **2** are  $8.36 \times 10^{27} \text{ m}^{-3} \text{ s}^{-1}$  ( $J_{ph, sat} = 134 \text{ A/m}^2$ ) and  $7.43 \times 10^{27} \text{ m}^{-3} \text{ s}^{-1}$  ( $J_{ph, sat} = 122 \text{ A/m}^2$ ), respectively. It is noted here that  $G_{max}$  is the maximum number of absorbed photons and such enhancement corresponds to the increased light absorption in the device based on **1** and consistent with absorption spectra of the **1**. The photocurrent density can be expressed as [73, 74]

$$J_{ph}(V) = P_{in} \eta_A \eta_{ED} \eta_{CT} P_C(V)$$

Where  $V$  is the applied voltage across the device,  $P_{in}$  is the incident light intensity,  $\eta_A$  is the absorption efficiency of photons in the active layer,  $\eta_{ED}$  exciton diffusion efficiency, which is the efficiency for the photogenerated excitons to diffuse to the D-A interfaces,  $\eta_{CT}$  is the charge transfer efficiency, which is related to the LUMO off set between the donor and acceptor materials used in the BHJ active layer, and  $P_C(V)$  is the charge collection efficiency, i.e. probability of charge collection of the separated carriers. The charge collection probability is voltage dependent. The  $P_C(V)$  can be expressed as [75]

$$P_C(V) = J_{ph}(V) / J_{ph, sat}$$

Under short circuit conditions,  $P_C(0)$  is equal to  $J_{sc}/J_{ph, sat}$ , and the values of  $P_C(0)$  for the device based on **1** and **2** are 0.89 and 0.83, respectively. The higher value of charge collection probability is attributed to the more favorable nanoscale morphology of the **1**:PC<sub>71</sub>BM active layer.

#### 4. Conclusions

In summary, we have designed and synthesized two low band gap small molecules **DRT3-BDT (1)** and **DTT3-BDT (2)** comprising of same BDT central core (donor) and different end capped acceptor units, i.e. rhodanine with ethyl hexyl and thiazolidione with ethylhexyl via linked an alkyl-substituted terthiophene (3T)  $\pi$ -conjugation bridge, respectively and used them as electron donor along with PC<sub>71</sub>BM as electron acceptor for BHJ small molecule solar cells. These devices showed quite reasonable high  $V_{oc}$  attributed to

their deeper HOMO energy levels. The optimized devices (processed with 3 v % DIO/ CF) based on **1**:PC<sub>71</sub>BM and **2**:PC<sub>71</sub>BM active layer yielded PCE of 6.76 % and 5.26%, respectively. The higher value of PCE for former device has been attributed to the more appropriate nanoscale morphology of active layer and balanced charge transport than the latter device.

### Acknowledgements

EP would like to thank MINECO for the project CTQ2013-47183-R and the support through Severo Ochoa Excellence Accreditation 2014-2018(SEV-2013-0319). We also thankful to Material Science laboratory, MNIT, Jaipur and Department of Physics, LNMIT, Jaipur for the availability of device fabrication facilities and other characterization.

### References

1. G. Dennler, M. C. Scharber and C. J. Brabec, *Adv. Mater.*, 2009, **21**, 132
2. P. M. Beaujuge and J. M. J. Fréchet, *J. Am. Chem. Soc.*, 2011, **133**, 20009;
3. G. Li, R. R. Zhu and Y. Yang, *Nat. Photonics* 2012, **6**, 153
4. S. Günes, H. Neugebauer and N. S. Sariciftci, *Chem. Rev.*, 2007, **107**, 1324.
5. A. Facchetti, *Chem. Mater.*, 2011, **23**, 733
6. B. Walker, C. Kim and T.-Q. Nguyen, *Chem. Mater.*, 2011, **23**, 470
7. J. Roncali, *Acc. Chem. Res.*, 2009, **42**, 1719.
8. G. Yu, J. Gao, J. C. Hummelen, F. Wudl and A. J. Heeger, *Science*, 1995, **270**, 1789
9. Y. J. Cheng, S. H. Yang and C. S. Hsu, *Chem. Rev.*, 2009, **109**, 5868
10. F.C. Krebs, *Sol. Energy Mater. Sol. Cells*, 2009, **93**, 394
10. T.D. Nielsen, C. Cruickshank, S. Foged, J. Thorsen and F.C. Krebs, *Sol. Energy Mater. Sol. Cells* 2010, **94**, 1553
11. H. Hoppe and N.S. Sariciftci, *J. Mater. Chem.*, 2006, **16**, 45
12. M. Helgesen, R. Søndergaard and F.C. Krebs, *J. Mater. Chem.*, 2010, **20**, 36
13. W. Cao and J. Xue, *Energy Environ. Sci.*, 2014, **7**, 2123.

14. Z. C. He, C. M. Zhong, S. J. Su, M. Xu, H.B. Wu and Y. Cao, *Nat. Photonics*, 2012, **6**, 591
15. W.-Y. Wong and C.-L. Ho, *Acc. Chem. Res.*, 2010, **43**, 1246
16. Z. C. He, C. M. Zhong, X. Huang, W.-Y. Wong, H. B. Wu, L. W. Chen, S. J. Su and Y. Cao, *Adv. Mater.*, 2011, **23**, 4636
17. J. You, L. Dou, K. Yoshimura, T. Kato, K. Ohya, T. Moriarty, K. Emery, C. C. Chen, J. Gao, G. Li and Y. Yang, *Nat. Commun.* 2013, **4**, 1446
18. S. Liu, K. Zhang, J. Lu, J. Zhang, H.-L. Yip, F. Huang, and Y. Cao, *J. Am. Chem. Soc.* 2013, **135**, 15326.
19. M. T. Lloyd, J. E. Anthony, G. G. Malliaras, *Mater. Today* 2007, **11**, 34
20. D. H. Wang, A. K. K. Kyaw, V. Gupta, G. C. Bazan and A. J. Heeger, *Adv. Energy Mater.*, 2013, **3**, 1161
21. J. Zhou, Y. Zuo, X. Wan, G. Long, Q. Zhang, W. Ni, Y. Liu, Z. Li, G. He, C. Li, B. Kan, M. Li and Y. Chen, *J. Am. Chem. Soc.*, 2013, **135**, 8484
22. Y. Liu, C. Chen, Z. Hong, J. Gao, Y. M. Yang, H. Zhou, L. Dou, G. Li and Y. Yang, *Sci. Rep.*, 2013, **3**, 3356
23. Y. Chen, X. Wan and G. Long, *Acc. Chem. Res.*, 2013, **46**, 2645
24. A. Mishra and P. Bauerle, *Angew. Chem., Int. Ed.*, 2012, **51**, 2020
25. J. E. Coughlin, Z. B. Henson, G. C. Welch and G. C. Bazan, *Acc. Chem. Res.*, 2014, **47**, 257.
26. Y. Lin, Y. Li and X. Zhan, *Chem. Soc. Rev.*, 2012, **41**, 4245
27. A. K. K. Kyaw, D. H. Wang, D. Wynands, J. Zhang, T.Q. Nguyen, G.C. Bazan and A. J. Heeger, *Nano Lett.*, 2013, **13**, 3796
28. B. Kan, Q. Zhang, M. Li, X. Wan, W. Ni, G. Long, Y. Wang, X. Yang, H. Feng, Y. Chen, *J. Am. Chem. Soc.* 2014, **136**, 15529
29. Y. Liu, C. Chen, Z. Hong, J. Gao, Y. Yang, H. Zhou, L. Dou, G. Li and Y. Yang, *Sci. Rep.*, 2013, **3**, 3356
30. B. Walker, C. Kim and T. Q. Nguyen, *Chem. Mater.*, 2011, **23**, 470
31. J. Min, Y. N. Luponosov, T. Ameri, A. Elschner, S. M. Peregudova, D. Baran, T. Heumuller, N. Li, F. Machui, S. Ponomarenko and C. J. Brabec, *Org. Electron.*, 2013, **14**, 219

32. J. Min, Y. N. Luponosov, A. Gerl, M. S. Polinskaya, S. M. Peregudova, P. V. Dmitryakov, A. V. Bakirov, M. A. Shcherbina, S. N. Chvalun, S. Grigorian, N. K. Busies, S. A. Ponomarenko, T. Ameri and C. J. Brabec, *Adv. Energy Mater.*, 2014, **4**, 1301234
33. J. Min, Y. N. Luponosov, Z.-G. Zhang, S. A. Ponomarenko, T. Ameri, Y. F. Li and C. J. Brabec, *Adv. Energy Mater.*, 2014, DOI: 10.1002/aenm.201400816
34. Y. Z. Lin, L. C. Ma, Y. F. Li, Y. Q. Liu, D. B. Zhu and X. W. Zhan, *Adv. Energy Mater.*, 2013, **3**, 1166
35. Y. M. Sun, G. C. Welch, W. L. Leong, C. J. Takacs, G. C. Bazan and A. J. Heeger, *Nat. Mater.*, 2012, **11**, 44
36. Y. S. Liu, Y. Yang, C. C. Chen, Q. Chen, L. T. Dou, Z. R. Hong, G. Li and Y. Yang, *Adv. Mater.*, 2013, **25**, 4657
37. J. Y. Zhou, X. J. Wan, Y. S. Liu, Y. Zou, Z. Li, G. R. He, G. K. Long, W. Ni, C. X. Li, X. C. Su and Y. S. Chen, *J. Am. Chem. Soc.*, 2012, **134**, 16345.
38. J. Min, Z. G. Zhang, S. Zhang and Y. Li, *Chem. Mater.*, 2012, **24**, 3247
39. L. Dou, J. Gao, E. Richard, J. You, C. C. Chen, K. C. Cha, Y. He, G. Li and Y. Yang, *J. Am. Chem. Soc.*, 2012, **134**, 10071
40. W. Li, W. S. Roelofs, M. M. Wienk and R. A. Janssen, *J. Am. Chem. Soc.*, 2012, **134**, 13787.
41. L. Huo, J. Hou, S. Zhang, H. Y. Chen and Y. Yang, *Angew. Chem., Int. Ed.*, 2010, **49**, 1500
42. Z. Du, W. Chen, Y. Chen, S. Qiao, X. Bao, S. Wen, M. Sun, L. Han and R. Yang, *J. Mater. Chem. A* 2014, **2**, 15904
43. Y. Huang, X. Guo, F. Liu, L. Huo, Y. Chen, T. P. Russell, C. C. Han, Y. Li and J. Hou, *Adv. Mater.*, 2012, **24**, 3383
44. D. Lee, E. Hubijar, G. J. D. Kalaw and J. P. Ferraris, *Chem. Mater.*, 2012, **24**, 2534
45. Y. Li, *Acc. Chem. Res.*, 2012, **45**, 723
46. M. Zhang, Y. Gu, X. Guo, F. Liu, S. Zhang, L. Huo, T. P. Russell and J. Hou, *Adv. Mater.*, 2013, **25**, 4944
47. J. Zhou, X. Wan, Y. Liu, Y. Zuo, Z. Li, G. He, G. Long, W. Ni, C. Li, X. Su and Y. Chen, *J. Am. Chem. Soc.*, 2012, **134**, 16345
48. D. Patra, T.Y. Huang, C. C. Chiang, R. O. V Maturana, C. W. Pao, K.C. Ho, K. H. Wei and C. W. Chu, *ACS Appl. Mater. Interfaces* 2013, **5**, 9494

49. J. Zhou, X. Wan, Y. Liu, G. Long, F. Wang, Z. Li, Y. Zuo, C. Li and Y. Chen, *Chem. Mater.*, 2011, **23**, 4666
50. D. Ye, X. Li, L. Xan, W. Zhang, Z. Hu, Y. Liang, J. Fang, W. Y. Wong and X. Wang, *J. Mater. Chem. A* 2013, **1**, 7622
51. C. C. Patra, W. A. Chiang, K. H. Chen, M.C. Wei, M.C. Wu and C.W. Chu, *J. Mater. Chem. A* 2013, **1**, 7767.
52. W. Ni, M. Li, X. Wan, H. Feng, B. Kan, Y. Zuo and Y. Chen, *RSC Adv.*, 2014, **4**, 31977
53. K. Sun, Z. Xiao, S. Lu, W. Zajaczkowski, W. Pisula, E. Hanssen, J. M. White, R. M. Williamson, J. Subbiah, J. Ouyang, A. B. Holmes, W. W. H. Wong and D. J. Jones, *Nat. Commun.* 6, 6013 doi:10.1038/ncomms7103 (2015)
54. Ch. V. Kumar, L. Cabau, E.N. Koukaras, A. Viterisi, G. D. Sharma, E. Palomares, J. Mater. Chem. A doi: 10.1039/c4ta05807k
55. J. P. Perdew, K. Burke, M. Ernzerhof, *Phys. Rev. Lett.* 1996, **77**, 3865.
56. A. Schafer, H. Horn and R. Ahlrichs, *J. Chem. Phys.* 1992, **97**, 2571.
57. K. Eichkorn, Q. Treutler, H. Öhm, M. Häser, R. Ahlrichs, *Chem. Phys. Lett.* 1995, **240**, 283.
- 58 A. D. Becke, *J. Chem. Phys.* 1993, **98**, 5648
59. C. Lee, W. Yang and R.G. Parr, *Phys. Rev. B* 1988, **37**, 785.
60. Y. Zhao and D.G. Truhlar, *Theor. Chem. Acc.* 2008, **120**, 215
61. Frisch, M. J.; Trucks, G. W.; Schlegel, H. B.; Scuseria, G. E.; Robb, M. A.; Cheeseman, J. R.; Scalmani, G.; Barone, V.; Mennucci, B.; Petersson, G. A.; Nakatsuji, H.; Caricato, M.; Li, X.; Hratchian, H. P.; Izmaylov, A. F.; Bloino, J.; Zheng, G.; Sonnenberg, J. L.; Hada, M.; Ehara, M.; Toyota, K.; Fukuda, R.; Hasegawa, J.; Ishida, M.; Nakajima, T.; Honda, Y.; Kitao, O.; Nakai, H.; Vreven, T.; Montgomery, Jr., J. A.; Peralta, J. E.; Ogliaro, F.; Bearpark, M.; Heyd, J. J.; Brothers, E.; Kudin, K. N.; Staroverov, V. N.; Kobayashi, R.; Normand, J.; Raghavachari, K.; Rendell, A.; Burant, J. C.; Iyengar, S. S.; Tomasi, J.; Cossi, M.; Rega, N.; Millam, J. M.; Klene, M.; Knox, J. E.; Cross, J. B.; Bakken, V.; Adamo, C.; Jaramillo, J.; Gomperts, R.; Stratmann, R. E.; Yazyev, O.; Austin, A. J.; Cammi, R.; Pomelli, C.; Ochterski, J. W.; Martin, R. L.; Morokuma, K.; Zakrzewski, V. G.; Voth, G. A.; Salvador, P.; Dannenberg, J. J.; Dapprich, S.; Daniels, A. D.; Farkas, Ö.; Foresman, J. B.; Ortiz, J. V.; Cioslowski, J.; Fox, D. J. Gaussian 03, revision C.01; Gaussian, Inc.: Wallingford CT, 2004.
62. TURBOMOLE (version 5.6); Universitat Karlsruhe, 2000.
63. D. Jacquemin, E.A. Perpète, I. Ciofini, R. Adamo Valero, Y. Zhao and D.G. Truhlar, *J. Chem. Theory Comput.* 2010, **6**, 2071.

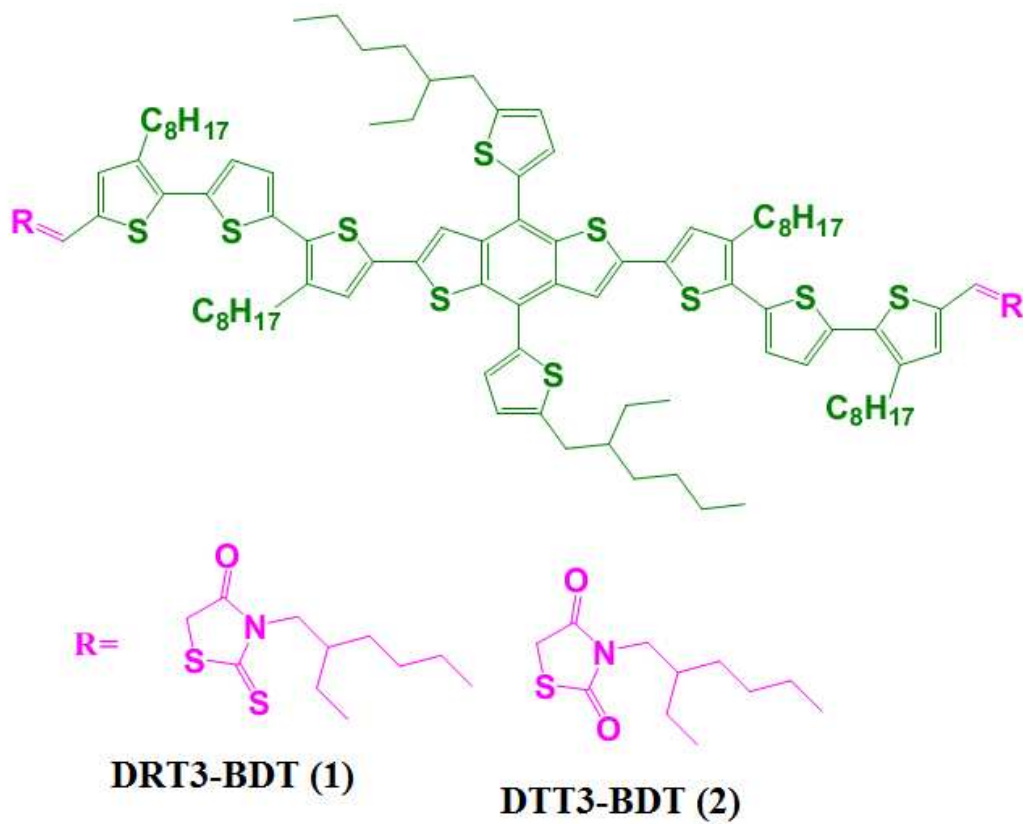
64. S. Mathew, A. Yella, P. Gao, R. Humphry-Baker, F.E. Curchod, N. Ashari-Astani, I. Tavernelli, U. Rothlisberger, M.K. Nazeeruddin and M. Grätzel, *Nature Chem.* 2014, **6**, 242
65. N. Lim, N. Cho, S. Paek, C. Kim, J. K. Lee and J. Ko, *Chem. Mater.* 2014, **26**, 2283
66. X. N. Yang, J. Loos, S.C. Veenstra, W. J. H. Verhees, M. M. Wienk, J. M. Kroon M.A. J. Michels, and R.A. J. Janssen, *Nano Lett.*, 2005, **5**, 579
67. J. E. Slota, X. He and W.T.S. Huck, *Nano Today* 2010, **5**, 231
68. J. Peet, M. L. Senatore, A. J. Heeger and G. C Bazan, *Adv. Mater.*, 2009, **21**, 1521
69. K. Schmidt, J. T. C.; J. R. Niskala, A.T. Yiu, O.P. Lee, T.M. Weiss, C. Wang, J.M.J. Fréchet, P.M. Beaujuge and M.F. Toney, *Adv. Mater.*, 2014, **26**, 300
70. D.H. Kim, A.L. Ayzner, A.L. Appleton, K. Schmidt, J.G. Mei, M.F. Toney and Z.A. Bao, *Chem. Mater.*, 2013, **25**, 431.
71. S. R. Cowan, A. Roy and A. J. Heeger, *Phys. Rev. B: Condens. Matter Mater. Phys.*, 2010, **82**, 245207.
72. V. D. Mihailetschi, H. X. Xie, B. de Boer, L. J. A. Koster and P. W. M. Blom, *Adv. Funct. Mater.*, 2006, **16**, 699.
73. R. A. Street, A. Krakaris and S. R. Cowan, *Adv. Funct. Mater.*, 2012, **22**, 4608
74. Z. He, C. Zhong, X. Huang, W.-Y. Wong, H. Wu, L. Chen, S. Su and Y. Cao, *Adv. Mater.*, 2011, **23**, 4636.
75. Z. Yi, W. Ni, Q. Zhang, M. Li, B. Kan, X. Wan and Y. Chen, *J. Mater. Chem. C* 2014, **3**, 7247

Table 1 Calculated properties of **DRT3-BDT (1)** and **DTT3-BDT (2)** molecules. Specifically HOMO and LUMO energies (eV), HOMO–LUMO gap (eV), HL, Optical gap (eV), OG, with corresponding oscillator strengths,  $f$ , the wavelengths of the first excitation and excitations with the largest oscillator strengths, the main contributions to the first excited state, and the dipole moment (D),  $\mu$

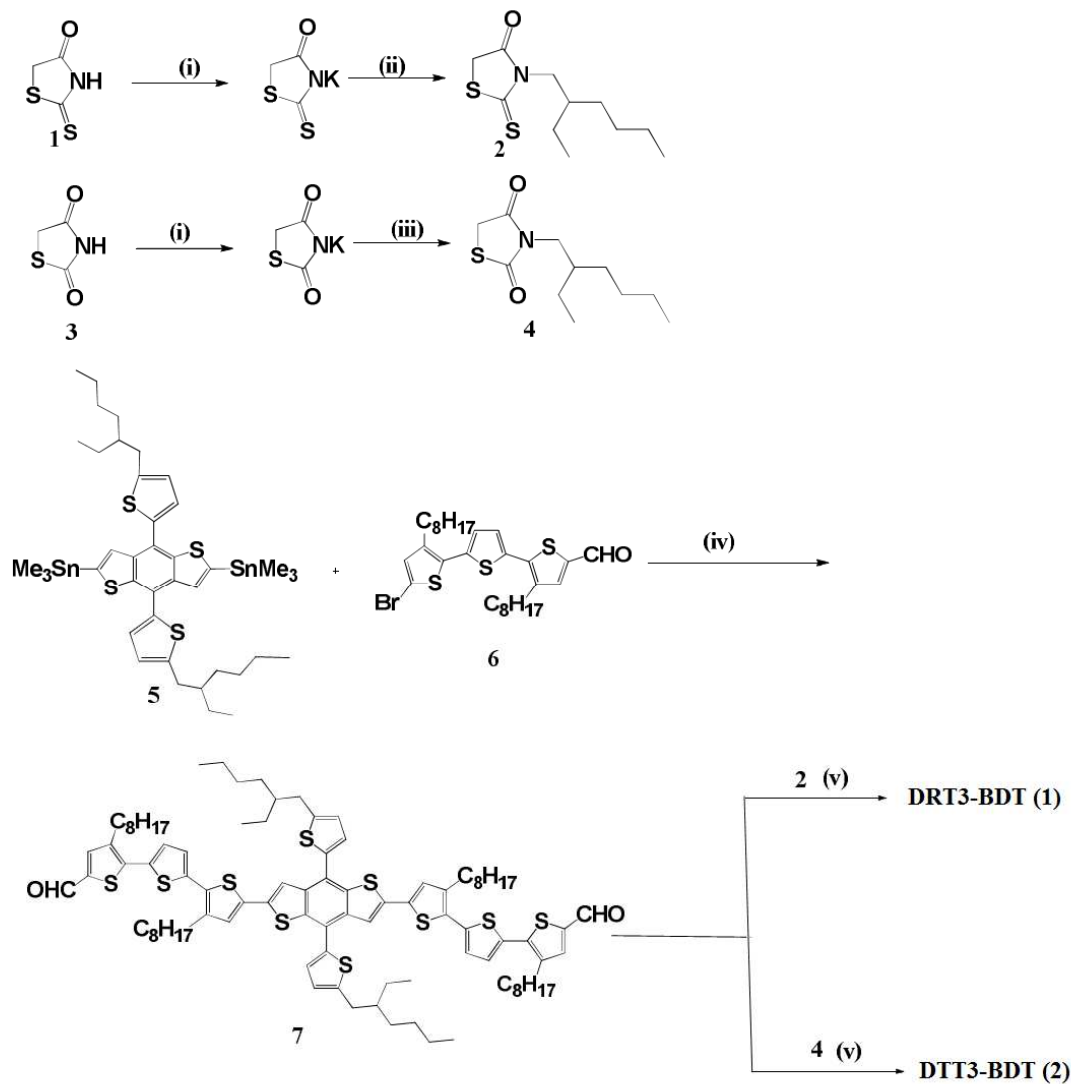
	HOMO O (eV)	LUMO (eV)	HL (eV)	OG (eV)	$\lambda_{1st/max}$ (nm)	$f$	Main Contributions	$\mu$ (D)
<b>DRT3-BDT (1)</b>								
<b>PBE</b>	-4.55	-3.40	1.15	1.25	990	0.95	H→L (91%), H-1→L+1 (5%)	2.20
<b>B3LYP</b>	-5.11	-2.90	2.21	1.95	637	2.83	H→L (94%)	2.03
<b>M06</b>	-5.37	-2.80	2.58	2.09	592	3.63	H→L (81%), H-1→L+1 (10%), H→L+2 (6%)	1.40
	-5.40 <sup>a</sup>	-2.85 <sup>a</sup>	2.54 <sup>a</sup>	2.02 <sup>a</sup>	613 <sup>a</sup>	3.96 <sup>a</sup>	H→L (77%), H-1→L+1 (13%), H→L+2 (6%) <sup>a</sup>	1.77 <sup>a</sup>
<b>DTT3-BDT (2)</b>								
<b>PBE</b>	-4.51	-3.28	1.23	1.36	914	1.00	H→L (89.8%), H-1→L+1 (5%)	2.50
<b>B3LYP</b>	-5.10	-2.74	2.35	2.07	599	2.81	H→L (95%)	2.93
<b>M06</b>	-5.38	-2.65	2.74	2.22	558	3.33	H→L (82%), H-1→L+1 (10%), H→L+2 (5%)	3.11
	-5.42 <sup>a</sup>	-2.69 <sup>a</sup>	2.72 <sup>a</sup>	2.16 <sup>a</sup>	574 <sup>a</sup>	3.68 <sup>a</sup>	H→L (79%), H-1→L+1 (12%), H→L+2 (5%) <sup>a</sup>	3.60 <sup>a</sup>

Table 2 Photovoltaic parameters of devices

Blends	$J_{sc}$ (mA/cm <sup>2</sup> )	$V_{oc}$ (V)	FF	PCE (%)
<b>1:PC<sub>71B</sub>M</b>	11.92	0.90	0.63	6.76
<b>2:PC<sub>71B</sub>M</b>	10.52	0.86	0.58	5.25



Scheme 1: Molecular structures of **DRT3-BDT (1)** and **DTT3-BDT (2)**



<sup>a</sup>Reaction conditions: (i).KOH,Ethanol,Reflux,5h; (ii) Ethyl hexyl bromide, KI, Acetone,DMF,36 h, 90° C; (iii) Ethyl hexyl bromide, DMF, Reflux, 4 h; (iv) Dry Toluene, Pd(PPh<sub>3</sub>)<sub>4</sub>,110°C 48 h; (v) Dry Chloroform, Pipperrine Reflux, 12-48 h

Scheme 2: Synthetic route of **DRT3-BDT (1)** and **DTT3-BDT (2)**<sup>a</sup>

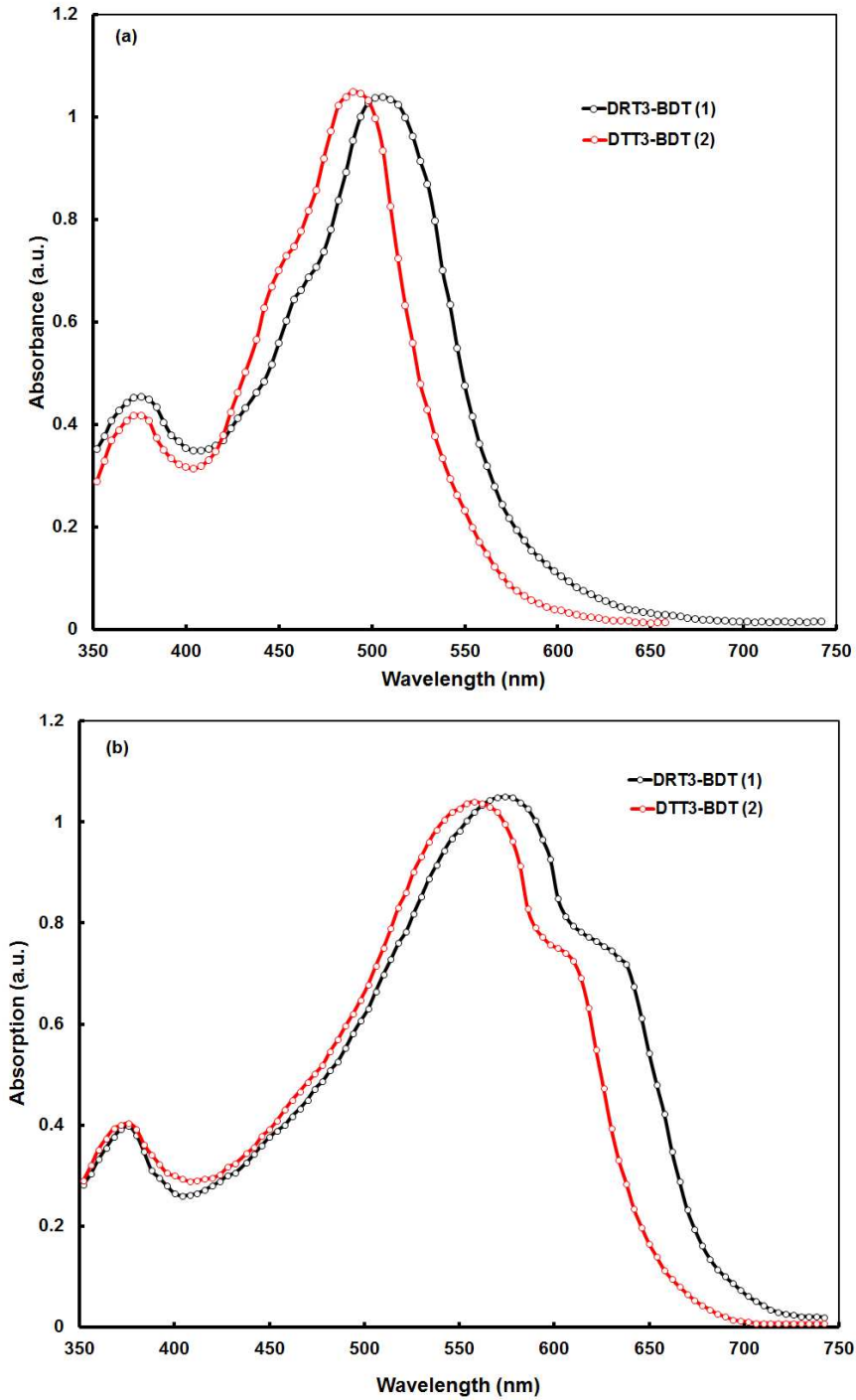


Figure 1 Optical absorption spectra of **DRT3-BDT (1)** and **DTT3-BDT (2)** in (a) chloroform solution and (b) thin film cast from chloroform solution

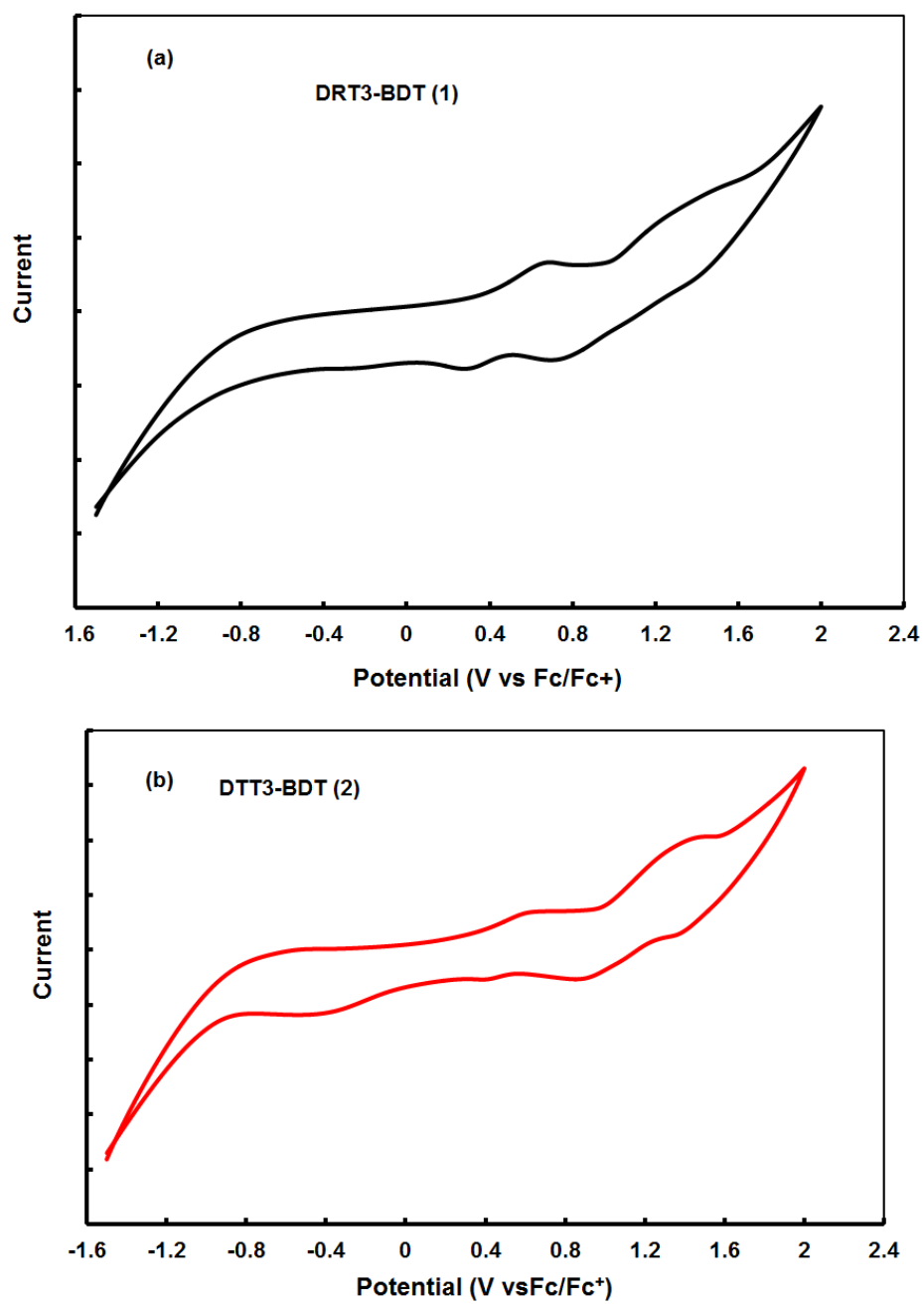


Figure 2 Cyclic voltammetry of **DRT3-BDT (1)** and **DTT3-BDT (2)**

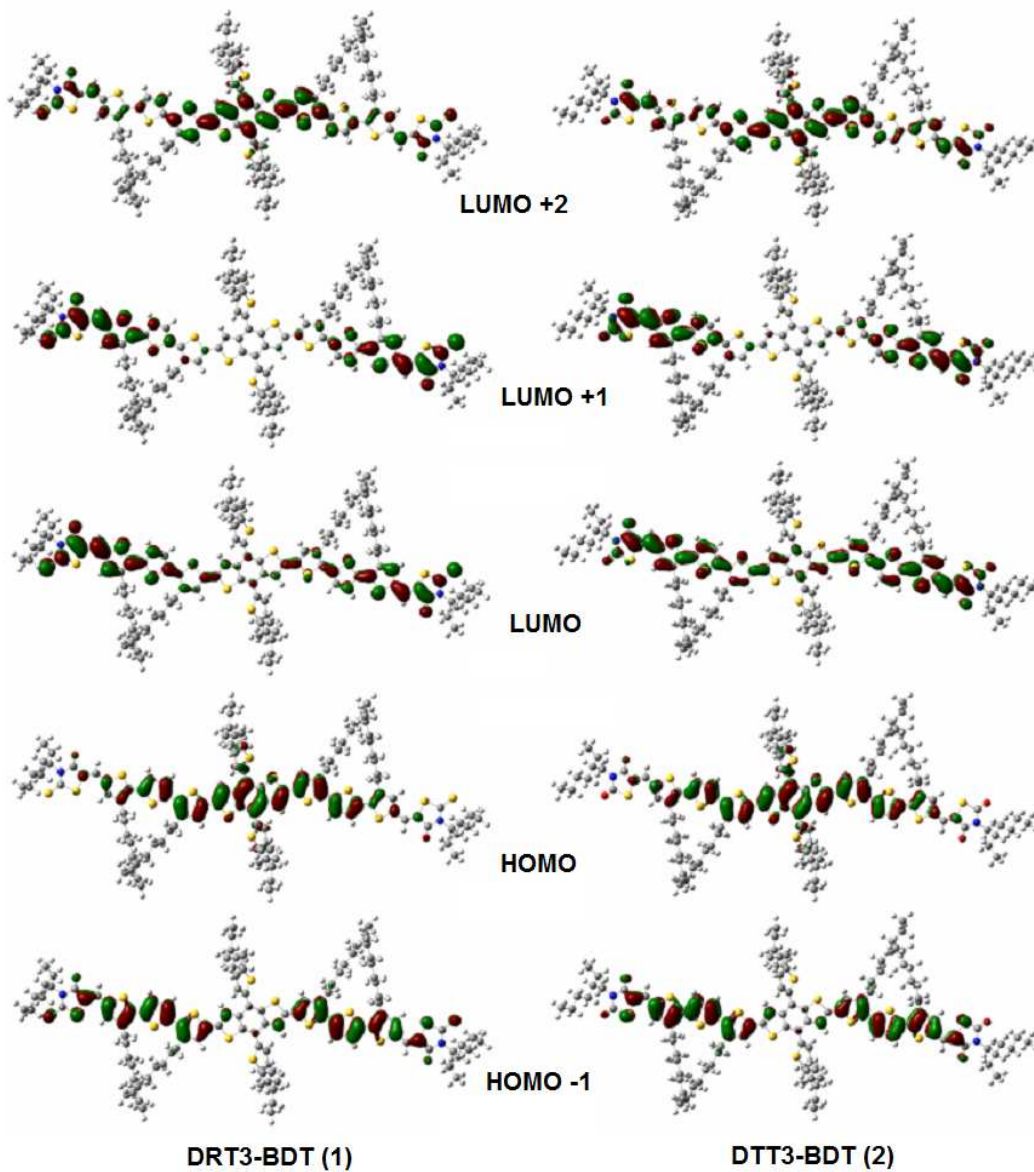


Figure 3 Frontier and near frontier orbitals of the (left) **DRT3-BDT (1)** and (right) **DTT3-BDT (2)** molecules.

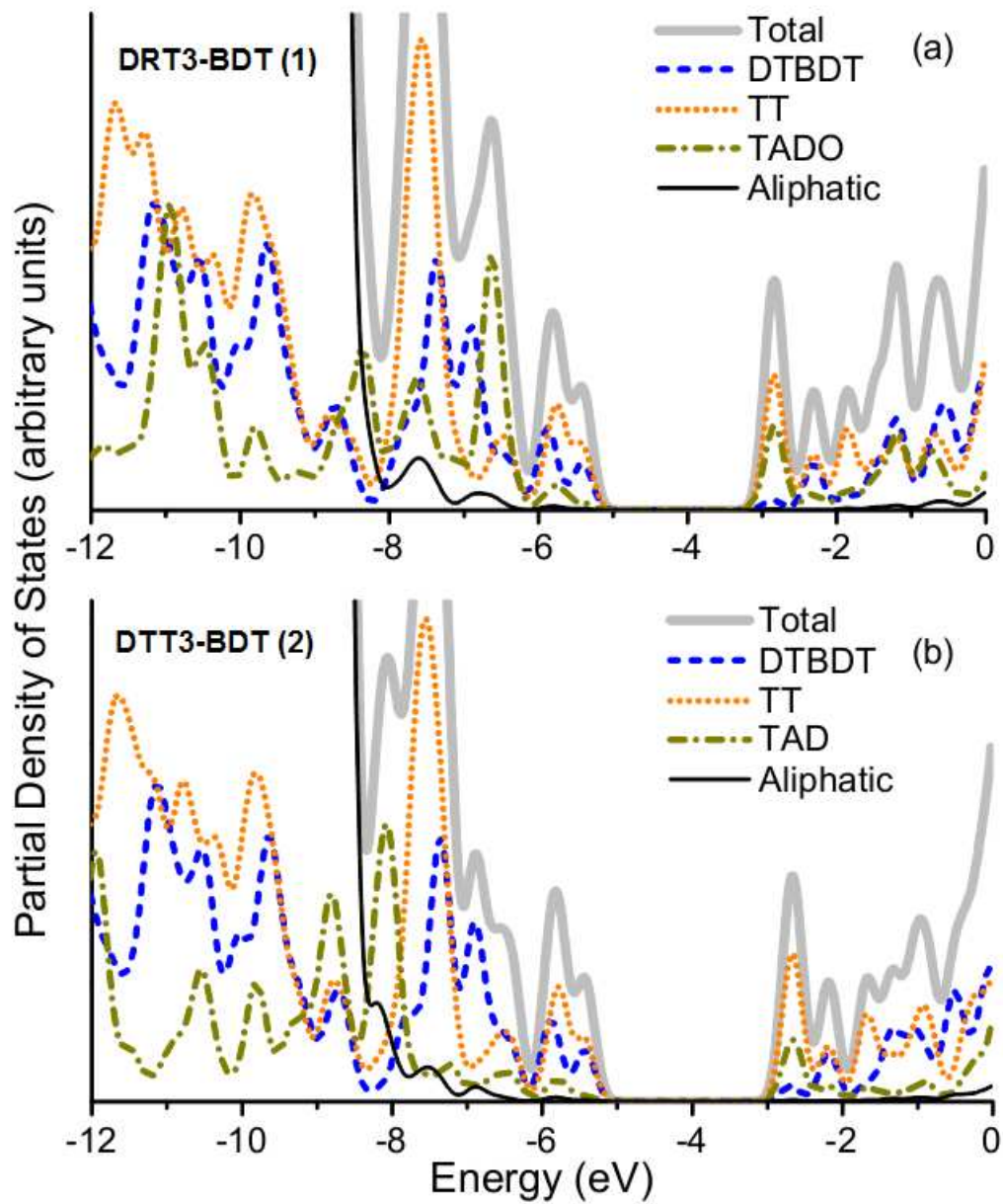


Figure 4 Total and partial density of states of the (a) **DRT3-BDT (1)** and (b) **DTT3-BDT (2)** molecules (calculated using the M06 functional)

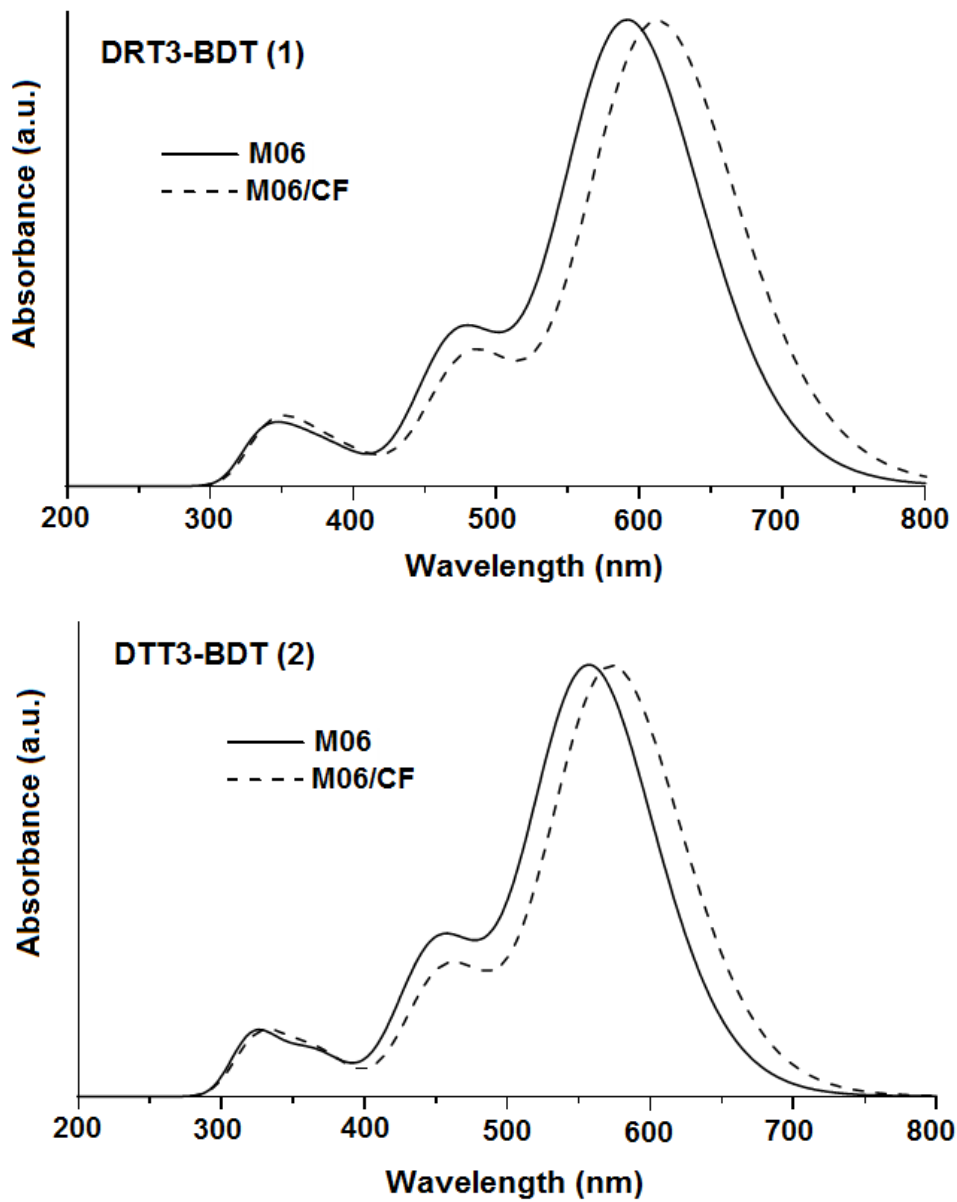


Figure 5 Theoretical UV/Vis absorption spectrum of (a) **DRT3-BDT (1)** and (b) **DTT3-BDT (2)** (calculated using the M06 functional).

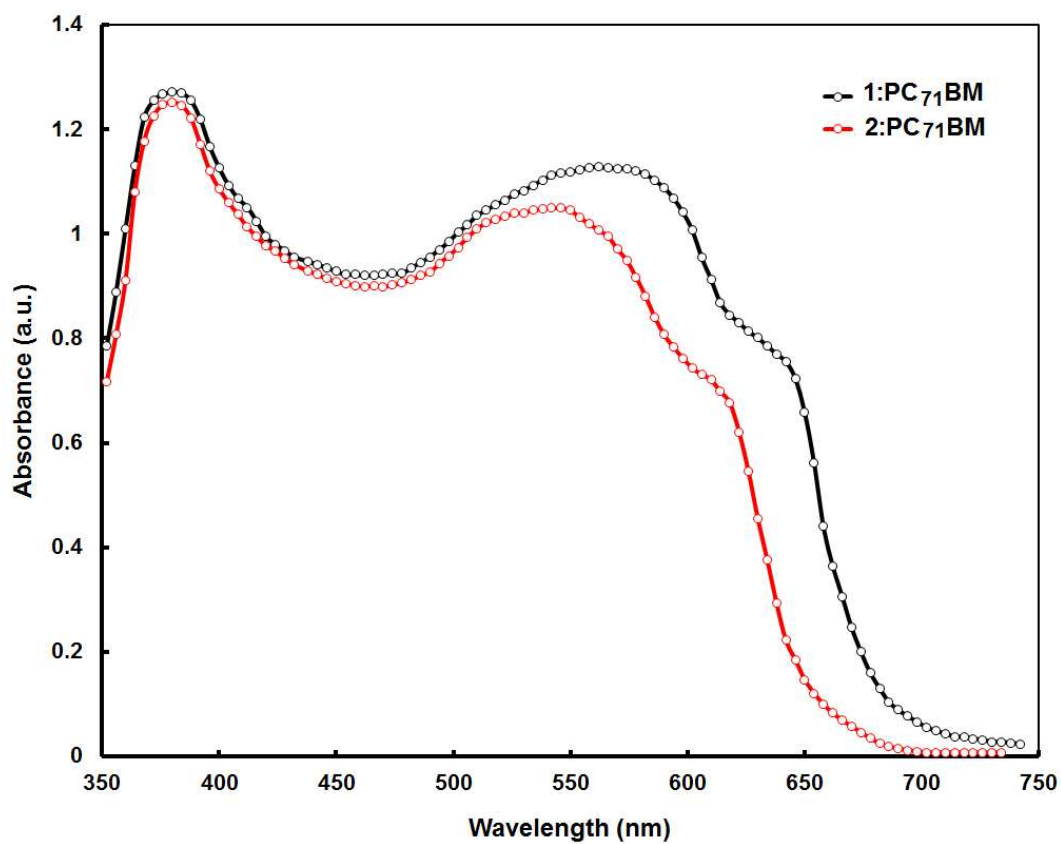


Figure 6 Normalized UV-vis absorption spectra of the 1 or 2:PC<sub>71</sub>BM (1:1) thin films cast from DIO/CF.

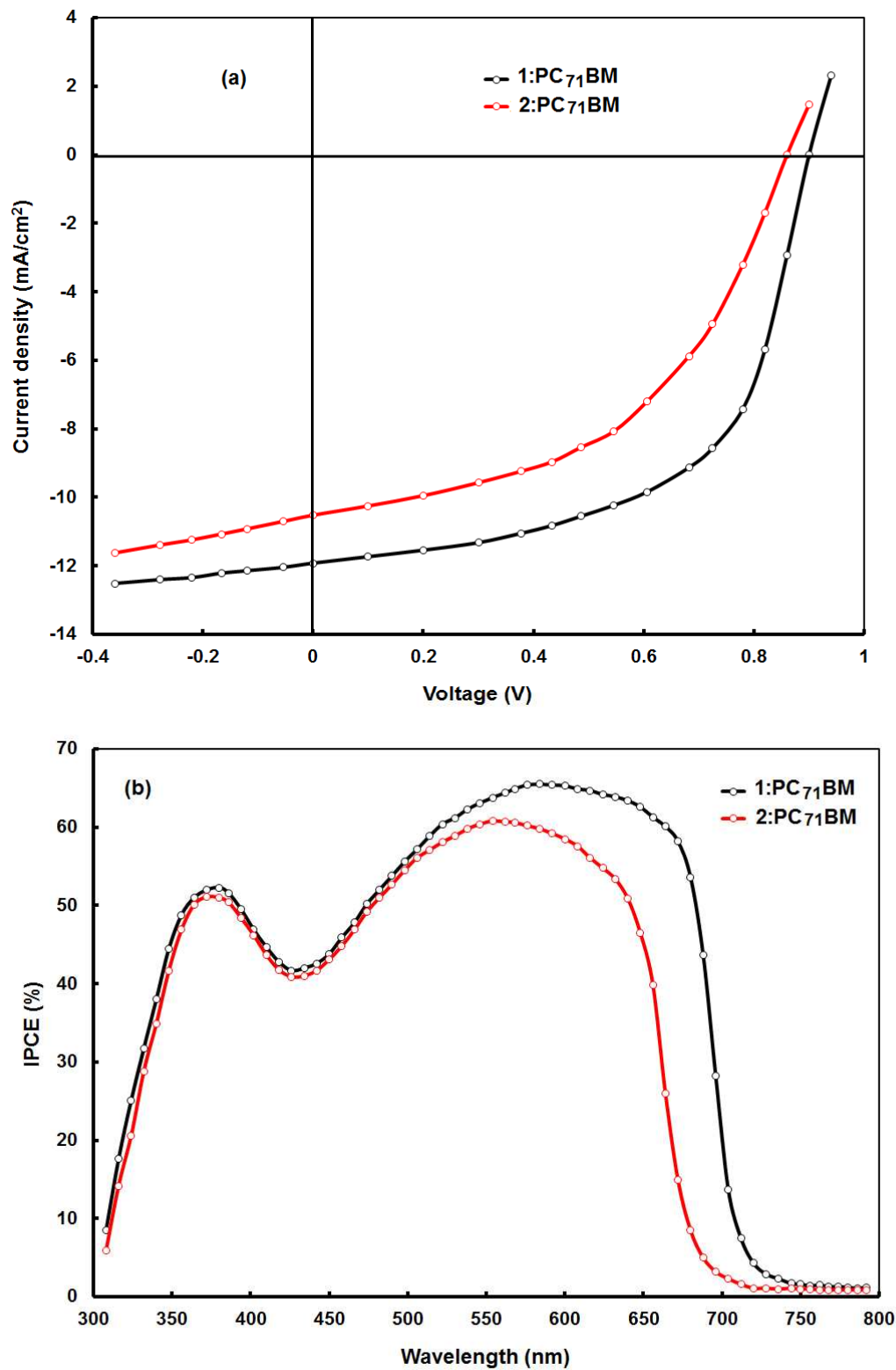


Figure 7 (a) Current- voltage (J-V) characteristics under illumination and (b) IPCE spectra of BHJ small molecule solar cells using **1** or **2**:PC<sub>71</sub>BM processed with DIO/CF solvents.

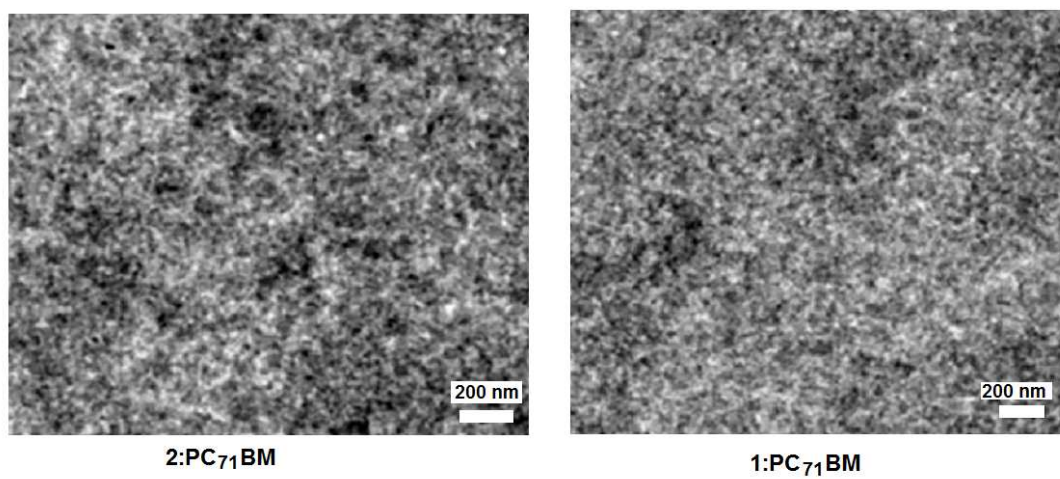


Figure 8 TEM images of 1:PC<sub>71</sub>BM and 2:PC<sub>71</sub>BM cast from DIO.THF

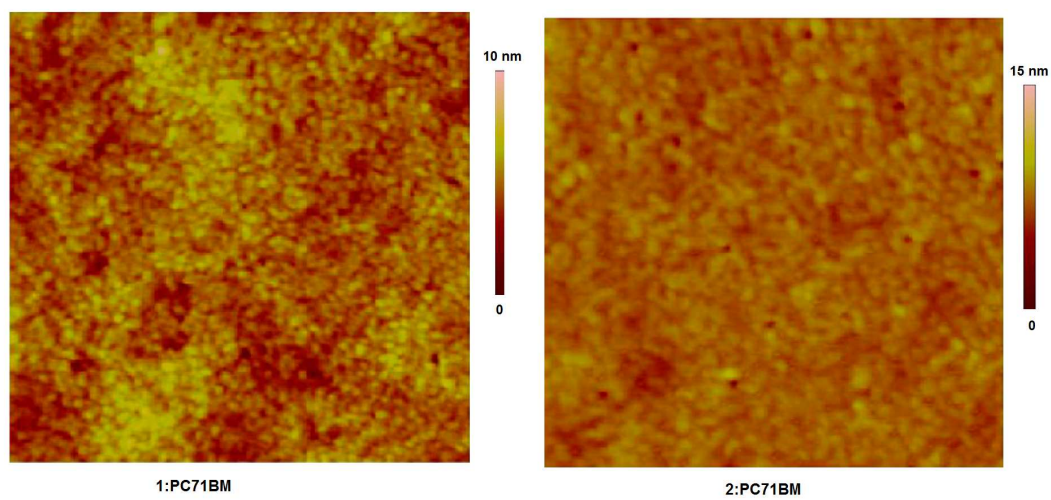


Figure 9 AFM images of 1:PC<sub>71</sub>BM and 2:PC<sub>71</sub>BM cast from DIO/CF solvent, image size 3 $\mu$ m

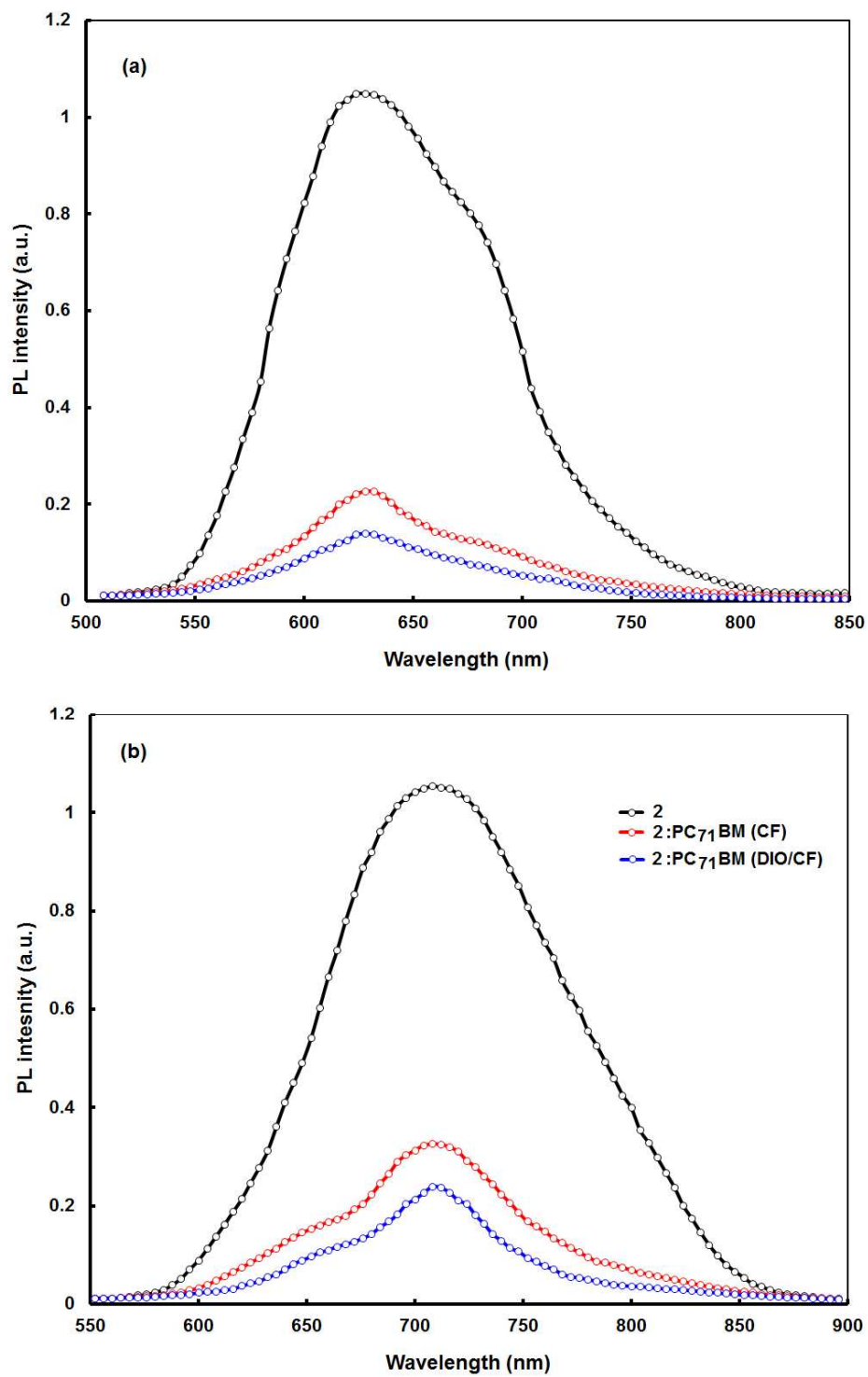


Figure 10 (a) Photoluminescence spectra of (a) **1** and **1:PC<sub>71</sub>BM** films and (b) **2** and **2:PC<sub>71</sub>BM** films spin-coated from solution without or with the 3 vol % DIO additive.

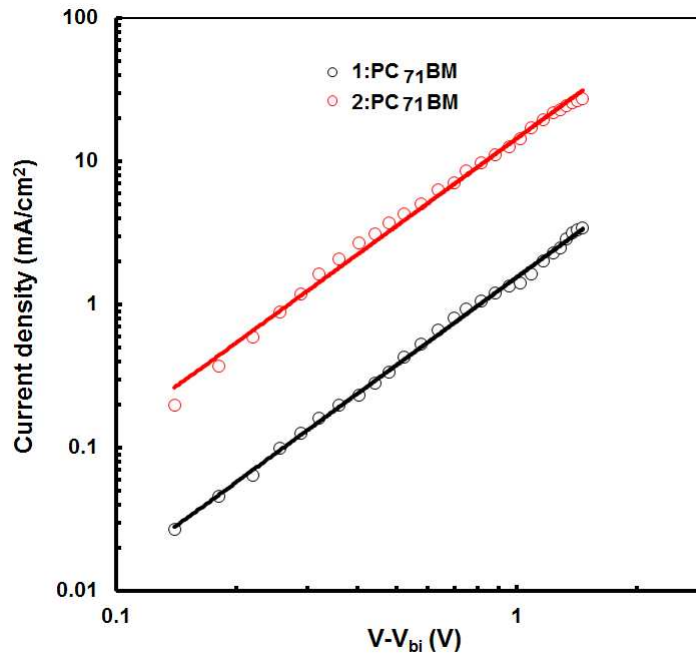


Figure 11 Variation of dark current density with  $V-V_{bi}$  for hole only devices. The solid lines indicate fits of experimental data that yields a slope of 2.

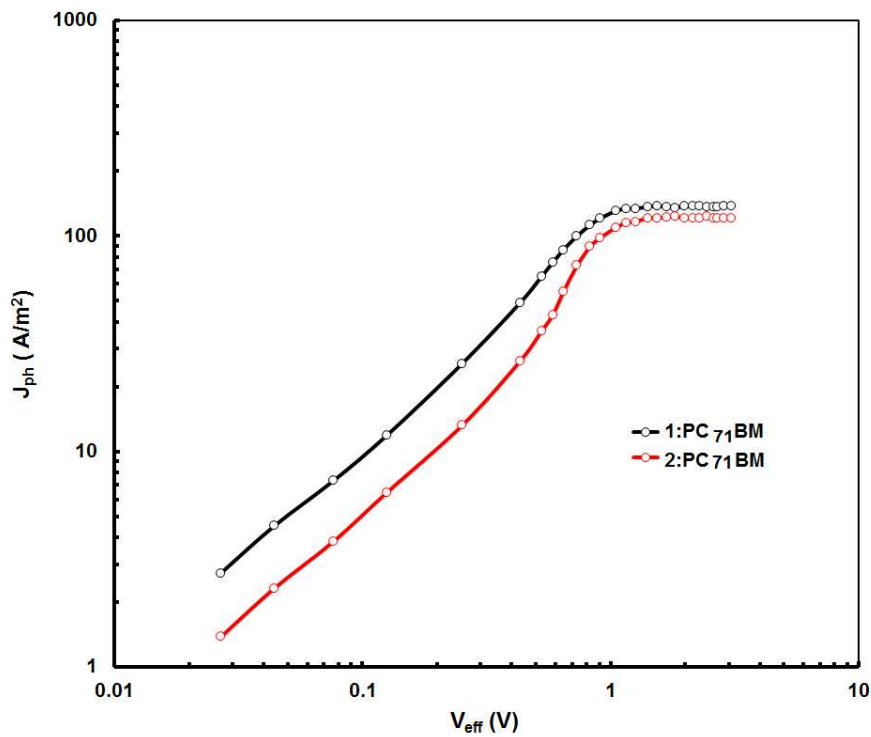


Figure 12 Variation of photocurrent density ( $J_{ph}$ ) as a function of effective voltage ( $V_{eff}$ ) for the devices